A

```
MDFLAPLAFLFSVASVSFAAADGSSEEGAKAVVELTEQNIHSYVAEHDAV   50
LVKFYAPWCMHCQSLAPEYEKAAKQLTEEGSEVILAELNCDSAPAVAQEF  100
GIEGYPTLKFFRHGTPRDYSGTRQAEGIVSWCKAVLLPAVVHVSSVADVP  150
EDADVTFVAVGYGAEDELMKEFESVADIHRNDASFYAIAGGEKAIYVVHK  200
GHDKFHFSGSTPADLVEFVQQESLPLFAEIGHSNYIRYFSSGKAISWFCS  250
LRADFEKYGATFAKVARALRSSVLFAWLDVEKFTAAKEAFAIESFPSVAH  300
QSPNGRYILAPEVYSFDDVEAVLRFYSDVEAGRVPRSIKSEEAPASNDGP  350
VVTLVGNTLPDFVKNATKPILLMVHSPFCEHCKKFMPAFTAFGETMGTSG  400
RVTVALLNGDGNESALDYIQWNAYPTVLLINPGSTEPIPFDGKRTVEELT  450
SFVDTHVPVEPHTEL                                      465
```

B

	Active-site I	Active-site II	C-terminal
B. caballi	APW**CMH**CQSL	SPF**CEH**CKKF	HTEL
T. gondii	APWCGHCKRM	APWCGYCKSF	GEEL
N. caninum	APWCGHCKRM	APWCGYCKSF	GEEL
P. falciparum	APWCGHCKRL	APWCGHCKKL	SEEL
C. parvum	APWCGHCTAL	AQWCGHCKNL	RDEL
L. major	APWCGHCKTL	APWCGHCKKL	EEDL
S. cerevisiae	APWCGHCKNM	APWCGHCKRL	HDEL
R. norvegicus	APWCGHCKAL	APWCGHCKQL	KDEL
H. sapiens	APWCGHCKAL	APWCGHCKQL	KEDL
	****.** .	...*..**	.*

C

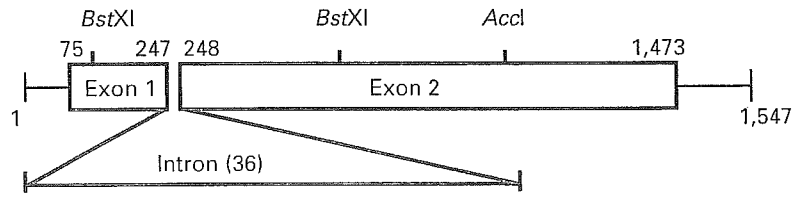

Fig. 1. (A) Deduced amino acid sequence of P51 (GenBank Accession no. AB201253). Numerical positions of amino acid sequences are indicated in the right margin, and predicted signal peptide residues are underlined. PDI and thioredoxin family active sites are underlined in bold. The probable ER retention sequence (HTEL) is in bold. (B) Amino acid sequence alignments of the putative active-site sequence of the PDI protein from *Toxoplasma gondii* (GenBank Accession no. AJ312317), *Neospora caninum* (GenBank Accession no. AB178220), *Plasmodium falciparum* (GenBank Accession no. AL844507), *Cryptosporidium parvum* (GenBank Accession no. BX538350), *Leishmania major* (GenBank Accession no. AY155573), *Saccharomyces cerevisiae* (Genbank Accession no. P17967), *Rattus norvegicus* (GenBank Accession no. P04785) and *Homo sapiens* (GenBank Accession no. P07237). Asterisks and dots below the sequence denote identical and similar amino acids, respectively. (C) Schematic representation of the genomic *p51* gene and *Bst* XI and *Acc* I restriction enzyme recognition sites in the *p51* gene. Nucleotide sequence of the intron is shown.

ORF encoded a protein of 465 amino acids which was 35·7% identical to the protein disulfide isomerase (PDI) of *Toxoplasma gondii* (GenBank Accession no. AJ3123), 34·6% identical to that of *Neospora caninum* (GenBank Accession no. AB178220), 32·0% identical to that of *Plasmodium falciparum* (GenBank Accession no. AL844507), 30·7% identical to that of *Cryptosporidium parvum* (Genbank Accession no. BX538350), and 26·5% identical to that of *Leishmania major* (GenBank Accession no. AY155573). The deduced amino acid sequence of the isolated clone exhibited an overall identity of 35·7–26·5% to proteins of PDI from several species. More specifically, this protein contained 2 distinct regions at 59–62 and 379–382 that are identical to the putative active-site sequence (Cys-X-X-Cys: CXXC) of the PDI (boldface and underlined in Fig. 1A and 1B). Moreover, the C-terminal peptides His-Thr-Glu-Leu (^{462}HTEL^{465}) may behave as an anchor to the endoplasmic reticulum (ER) (boldface in Fig. 1A and 1B). Based on these data, we concluded that we had isolated the *B. caballi* PDI gene.

Intron analysis of p51 *gene*

B. caballi genomic DNA was amplified by PCR using 1 set of oligonucleotide primers, Bcp51F and Bcp51R. The resulting DNA fragment was approx. 1600 nucleotides. The plasmid containing the gene was then isolated and subjected to DNA sequence analysis. The completed DNA sequence of the *p51* gene was analysed and found to contain a single intron of 36 nucleotides (Fig. 1C). The sequence of the splice junctions of this intron was similar to those found in other species of protozoan parasites, such as *P. falciparum* PDI (Florent *et al.* 2000).

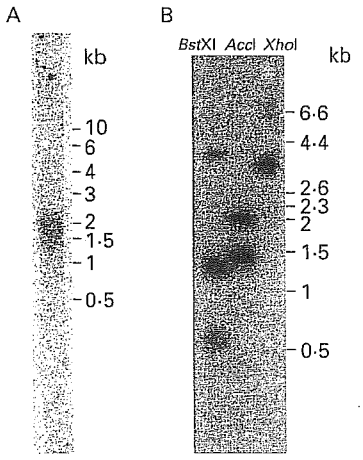

Fig. 2. (A) Northern blotting hybridization of the *p51* gene of *Babesia caballi*. Tracks contained 10 μg of total RNA prepared from *B. caballi*-infected erythrocytes and were hybridized with the ^{32}P-labelled *p51* cDNA. The size of the markers in kilo-bases is shown at right. (B) Southern blotting hybridization of the *p51* gene of *B. caballi*. Genomic DNA (10 μg per lane) from *B. caballi*-infected erythrocytes was digested with *Bst* XI, *Acc* I or *Xho* I, and hybridized with the ^{32}P-labelled *p51* cDNA. Size of the markers in base-pairs is shown at right.

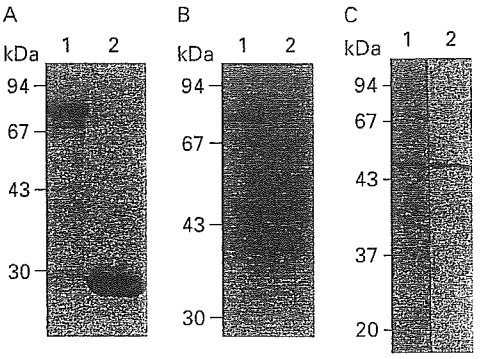

Fig. 3. Production of recombinant GST-P51 and Western blotting analysis of mAb 2H2 and anti-P51 antibody. (A) Recombinant protein samples were subjected to SDS-PAGE (10% acrylamide) and visualized by Coomassie Blue staining. Purification of recombinant GST-P51 protein (lane 1) and purified recombinant GST (lane 2). (B) Western blotting analysis of recombinant proteins, GST-P51 protein (lane 1) and GST (lane 2), probed with mAb 2H2. (C) Western blotting analysis of native *Babesia caballi*-infected erythrocytes with anti-P51 antibody (lane 1) and mAb 2H2 (lane 2). Molecular weights of markers in kDa are shown at left (Fig. A, B and C).

Characterization of P51 gene

A probe from a *p51* cDNA clone was hybridized to the total RNA isolated from *B. caballi* merozoite by Northern blotting. The mRNA of the *p51* gene is about 1·8 kb (Fig. 2A).

A probe derived from the *p51* cDNA clone was hybridized to *B. caballi* DNA fragments by Southern blotting. Genomic DNA was digested with the restriction enzymes *Xho* I, *Acc* I and *Bst* XI. The cDNA sequence, which did not contain a *Xho* I site, contained only a single *Acc* I site and 2 *Bst* XI sites (Fig. 1C). One band only was obtained on *Xho I* digestion, 2 on *Acc* I digestion, and 3 on *Bst* XI digestion (Fig. 2B). These results suggested that the *p51* gene occurs as a single copy in the genome of *B. caballi*.

Expression of p51 *in* E. coli *by pGEX-4T vector*

The *p51* gene was ligated into the bacterial expression vector pGEX-4T, and P51 was expressed as a fusion protein with the GST protein in *E. coli*. The molecular masses of the GST protein and GST-P51 fusion proteins were estimated to be 27 and 78 kDa, respectively, as expected (Fig. 3A and B). Moreover, antibodies against GST-PDI fusion protein from the mice recognized only the 51 kDa native protein as mAb 2H2 (Fig. 3C). These results indicate that this 51 kDa protein did not contain the epitope of other constituent proteins in *B. caballi* and was unique among these proteins.

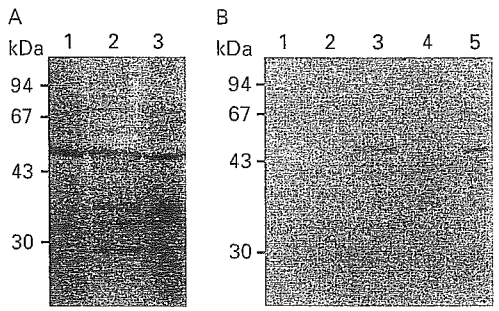

Fig. 4. Western blotting of recombinant AcP51 expressed in insect cells using anti-P51 antibody. (A) Lane 1: *Babesia caballi*-infected erythrocytes; lane 2: AcP51-His-infected insect cells; lane 3: AcP51-His-infected insect cell culture media. (B) Lane 1, non-infected insect cells; lane 2: non-infected insect cell culture media; lane 3: AcP51-stop-infected insect cells; lane 4: AcP51-stop-infected insect cell culture media; lane 5: *B. caballi*-infected erythrocytes. Molecular weights of markers in kDa are shown at left (Fig. A and B).

Expression of p51 *in insect cells by recombinant baculovirus*

Sf9 cells were infected at 5 PFU/cell with A*cp51*-His or A*cp51*-stop. After incubation for 3 days, cells infected with A*cp51*-His or A*cp51*-stop and culture media were analysed by Western blotting with anti-P51 antibody. As shown in Fig. 4, a single band of P51 protein was observed in the cell lysate with A*cp51*-His and with A*cp51*-stop, and in culture medium with A*cp51*-His, and the molecular mass

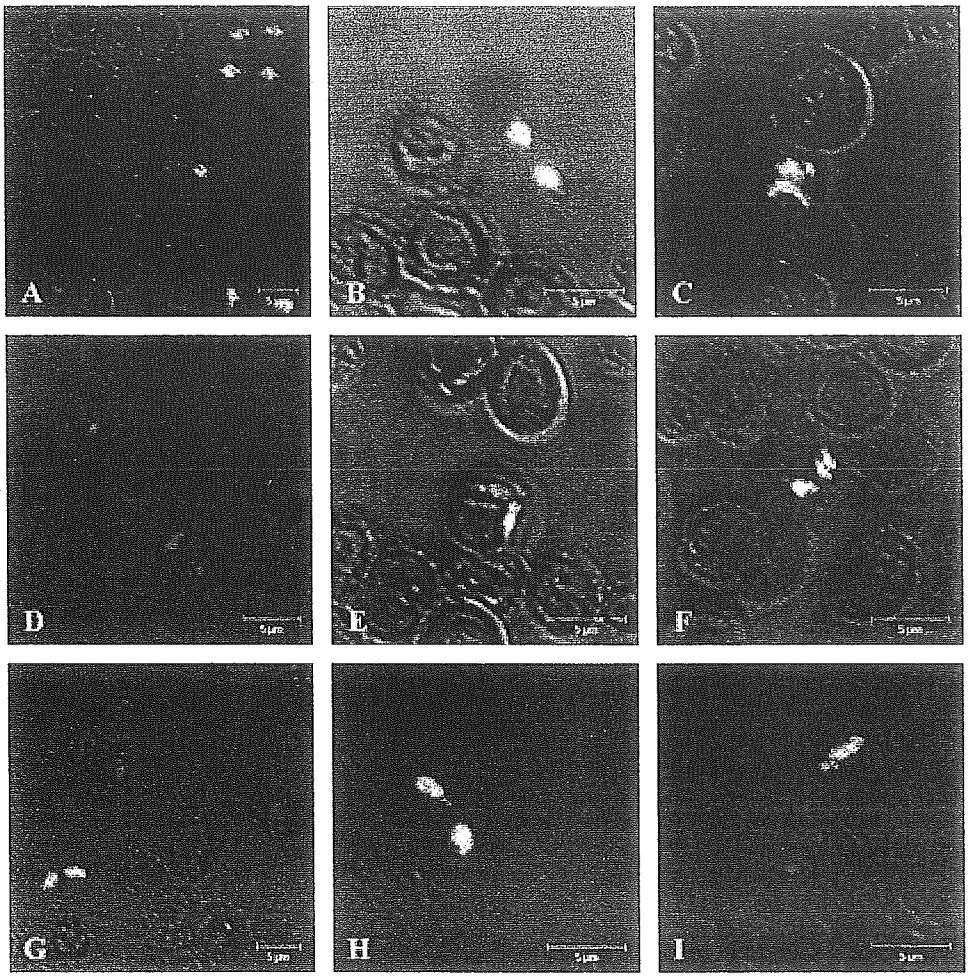

Fig. 5. Confocal laser micrograph of IFAT reactive patterns. Methanol-acetone-fixed smears of *Babesia caballi*-infected erythrocytes were incubated with anti-P51 antibody (A–F) and mAb 2H2 (G–I). Several extracellular *B. caballi* merozoites (positive reaction) and earlyphase of trophozoite (negative reaction) (A, B, G and H). Trophozoites reacted to anti-P51 antibody and mAb 2H2 (C and I). Anti-P51 antibody and mAb 2H2 were markedly irregular against pear-shaped forms, with either no reaction (D and I), reaction to 1 (E) or reaction to 2 (F). Positive reactions (green) and the parasites' nuclei (red) were visualized with FITC-conjugated goat anti-mouse IgG and propidium iodide (PI), respectively.

of the P51 protein was demonstrated to be the same as that of the native *B. caballi* 51-kDa protein by Western blotting (Fig. 4A, lanes 1 and 2; Fig. 4B, lane 3), suggesting that the ORF in the *p51* gene was the complete length. In contrast, no band was detected in the culture medium of A*cp51*-stop infected cells (Fig. 4B, lane 4). It remained possible that the putative ER-retention signal site (HTEL) of the recombinant protein was still functional in the ER of insect cells.

Cellular localization of B. caballi *P51*

In IFAT, the anti-P51 antibody and mAb 2H2 showed identical reactive patterns on the cold methanol-acetone-fixed preparations of *B. caballi* (Fig. 5). The anti-P51 antibody and mAb 2H2 reacted strongly with extracelluar *B. caballi* merozoites (Fig. 5A, B, G and H), and did not react in the early phase of trophozoite development (Fig. 5A and G). However, detailed observation showed that the reaction of anti-P51 antibody and mAb 2H2 were markedly irregular against pear-shaped forms, with either no reaction, or reaction to one or two brightly fluorescent pear-shaped forms (2 parasites) of *B. caballi* (Fig. 5D, E, F and I). Further, some trophozoites reacted to anti-P51 antibody (Fig. 5C and I). Moreover, the anti-P51 antibody reacted with the neighbourhood of the nucleus of extracellular and intracellular *B. caballi* merozoites (Fig. 5B and F).

DISCUSSION

As part of our efforts to identify new targets for chemotherapy against the parasite *B. caballi*, we identified the complete cDNA sequence of a highly expressed 51 kDa *B. caballi* extracellular merozoite

protein which displays all the structural features and consensus sequences expected for a typical PDI, and corresponds to P51 of *B. caballi*.

Following immunoscreening with the mAb 2H2, determination of the deduced amino acid sequence of the *p51* gene DNA showed homologies to the PDI of other species. The *p51* gene sequence in the *B. caballi* genome of a single copy gene contained an intron, the splice junction of which was similar to those found in *P. falciparum* PDI (Florent *et al.* 2000). Further, the P51 protein also conserved 2 PDI Cys (CXXC) motifs and the ER retention signal site of the C-terminal. Moreover, analysis of recombinant baculovirus expression of the *p51* gene in insect cells showed that its ER retention signal site was functional. In IFAT, the anti-P51 antibody reacted with the neighbourhood of the nucleus of extracellular and intracellular *B. caballi* merozoites. These results strongly suggest that the P51 protein is the PDI of *B. caballi*.

PDI is a member of the thioredoxin superfamily, which is composed of several redox proteins. It plays a key role in disulfide bond formation, isomerization and reduction within the ER, and also displays chaperone activity (Ferrari and Soling, 1999). PDI has 2 independent but non-equivalent active sites, each with 2 Cys (CXXC) that cycle between the dithiol and disulfide oxidation states, each within domains with high sequence similarity to thioredoxin (Vuori *et al.* 1992; Lyles and Gilbert, 1994). It is a highly abundant ER luminal protein in mammalian cells and yeast, and is essential in assisting unfolded or incorrectly folded proteins to attain their native state.

In general, PDI in eukaryotic cells have been described as having several isoforms as PDI family members. However, all of the members of the *B. caballi* PDI family and the mechanism by which *B. caballi* PDI affects the parasite in the process of invasion is also presently unknown and could not be determined in this study. Our rationale behind this search was that, from first attachment until completion of the invasion process, *B. caballi* secretes proteins from apical organelles into the merozoite membrane and into the environment; and that given that proteins secreted by apicomplexan parasites from micronemes, rhoptries and dense granules are generally thought to play a central role in invasion and the establishment of infection (Carruthers, 1999; Soldati *et al.* 2001), the adaptation of *B. caballi* at different stages of its development within host cells, and in the invasive process itself, may involve newly synthesized proteins or stress proteins. Therefore, one suggestion may be that *B. caballi* PDI plays an important role in host–parasite interactions, specifically in the optimal folding of proteins important for parasite inversion that are either secreted or expressed at the *B. caballi* parasite.

Support for this may come from the finding that a series of 1,4-bis (3-aminopropyl) piperazine compounds displays high activity in culture on *P. falciparum*, which is also one of the Apicomplexa. The homologue of the PDI of *P. falciparum* was isolated via a search for the plasmodial targets of this parasite by affinity chromatography using one of these compounds as a ligand (Florent *et al.* 2000). We therefore consider that the *B. caballi* PDI identified in the present study represents a new target for anti-*B. caballi* chemotherapy.

Moreover, mAb 2H2 recognized a 51 kDa protein produced by *B. caballi*. In IFAT, this protein was strongly expressed by extracellular *B. caballi* merozoites, and was little or not expressed in the early phase of trophozoite development. Interestingly, detailed observation showed that the expression of 51 kDa protein was markedly irregular, on fluorescence showing either no reaction, or one or two brightly fluorescent pear-shaped forms (2 parasites) of *B. caballi*. This result may suggest that the maturation of *B. caballi* merozoites after binary fission is not synchronous, and that the maturation process differs among individual merozoites.

In conclusion, the complete cDNA sequence isolated in this study encodes a protein displaying all the structural features and consensus sequences expected for a typical PDI, and corresponds to P51 of *B. caballi*. Further, the ER retention signal site (HTEL) of the recombinant protein retained its function in ER of insect cells. However, P51 of *B. caballi* was not conclusively identified as PDI in this study because we did not test the function of its protein. Thus, further studies are necessary to examine the function of this gene and the role of its protein in the process of invasion. In this regard, identification of PDI in *B. caballi* may facilitate the development of new inhibitors which, either independently or in conjunction with established therapies, may offer alternative treatments for *B. caballi* infection.

This study was supported by Grants-in-Aid for Scientific Research and Young Scientists from the Ministry of Education, Culture, Sports, Science and Technology of Japan and the Japan Society for the Promotion of Science, and the Kitasato University Research Grant for Young Researchers.

REFERENCES

Avarazed, A., Igarashi, I., Kanemaru, K., Hirumi, K., Omata, Y., Saito, A., Oyamada, T., Nagasawa, H., Toyoda, Y. and Suzuki, N. (1997). Improved *in vitro* cultivation of *Babesia caballi*. *Journal of Veterinary Medical Science* **59**, 479–481.

Blackman, M. J. and Bannister, L. H. (2001). Apical organelles of Apicomplexa: biology and isolation by subcellular fractionation. *Molecular and Biochemical Parasitology* **117**, 11–25.

Brüning, A. (1996). Equine piroplasmosis: an update on diagnosis, treatment and prevention. *British Veterinary Journal* **152**, 139–151.

Carruthers, V. B. (1999). Armed and dangerous: *Toxoplasma gondii* uses an arsenal of secretory proteins to infect host cells. *Parasitology International* **48**, 1–10.

Dubremetz, J. E., Garcia-Reguet, N., Conseil, V. and Fourmaux, M. N. (1998). Apical organelles and host-cell invasion by Apicomplexa. *International Journal for Parasitology* **28**, 1007–1013.

Feinberg, A. P. and Vogelstein, B. (1983). A technique for radiolabeling DNA restriction endonuclease fragments to high specific activity. *Analytical Biochemistry* **132**, 6–13.

Ferrari, D. M. and Soling, H. D. (1999). The protein disulfide-isomerase family: unravelling a string of folds. *Biometrical Journal* **339**, 1–10.

Florent, I., Mouray, E., Dali Ali, F., Drobecq, H., Girault, S., Schrevel, J., Sergheraert, C. and Grellier, P. (2000). Cloning of *Plasmodium falciparum* protein disulfide isomerase homologue by affinity purification using the antiplasmodial inhibitor 1,4-bis[3-[N-(cyclohexyl methyl)amino]propyl]piperazine. *FEBS Letters* **484**, 246–252.

Ikadai, H., Martin, M. D., Nagasawa, H., Fujisaki, K., Suzuki, N., Mikami, T., Kudo, N., Oyamada, T. and Igarashi, I. (2001). Analysis of a growth-promoting factor for *Babesia caballi* cultivation. *Journal of Parasitology* **87**, 1484–1486.

Ikadai, H., Tamaki, Y., Xuan, X., Igarashi, I., Kawai, S., Nagasawa, H., Fujisaki, K., Toyoda, Y., Suzuki, N. and Mikami, T. (1999*a*). Inhibitory effect of monoclonal antibodies on the growth of *Babesia caballi*. *International Journal for Parasitology* **29**, 1785–1791.

Ikadai, H., Xuan, X., Igarashi, I., Tanaka, S., Kanemaru, T., Nagasawa, H., Fujisaki, K., Suzuki, N. and Mikami, T. (1999*b*). Cloning and expression of a 48-kilodalton *Babesia caballi* merozoite rhoptry protein and potential use of the recombinant antigen in an enzyme-linked immunosorbent assay. *Journal of Clinical Microbiology* **37**, 3475–3480.

Knowles, R. C. (1998). Equine babesiosis: epidemiology, control and chemotherapy. *Equine Veterinary Science* **8**, 61–64.

Lyles, M. M. and Gilbert, H. F. (1994). Mutations in the thioredoxin sites of protein disulfide isomerase reveal functional nonequivalence of the N- and C-terminal domains. *Journal of Biological Chemistry* **269**, 30946–30952.

Preiser, P., Kaviratne, M., Khan, S., Bannister, L. and Jarra, W. (2000). The apical organelles of malaria merozoites: host cell selection, invasion, host immunity and immune evasion. *Microbe and Infection* **2**, 1461–1477.

Sambrook, J., Fritsch, E. F. and Maniatis, T. (1989). *Molecular Cloning: a Laboratory Manual*, 2nd Edn. Cold Spring Harbor Laboratory Press, Cold Spring Harbor, USA.

Schein, E. (1985). Equine babesiosis. In *Babesiosis of Domestic Animals and Man* (ed. Ristic, M.) pp. 197–208. CRC press, Boca Raton, Florida, USA.

Soldati, D., Dubremetz, J. F. and Lebrun, M. (2001). Microneme proteins: structural and functional requirements to promote adhesion and invasion by the apicomplexan parasite *Toxoplasma gondii*. *International Journal for Parasitology* **31**, 1293–1302.

Von Heijne, G. (1986). A new method for predicting signal sequence cleavage sites. *Nucleic Acids Research* **14**, 4683–4690.

Vuori, K., Myllyla, R., Pihlajaniemi, T. and Kivirikko, K. I. (1992). Expression and site-directed mutagenesis of human protein disulfide isomerase in *Escherichia coli*. This multifunctional polypeptide has two independently acting catalytic sites for the isomerase activity. *Journal of Biological Chemistry* **267**, 7211–7214.

Available online at www.sciencedirect.com
SCIENCE DIRECT®
Experimental Parasitology 110 (2005) 244–252
Experimental Parasitology
www.elsevier.com/locate/yexpr

The diversity of Rab GTPases in *Entamoeba histolytica* ☆

Yumiko Saito-Nakano [a], Brendan J. Loftus [b], Neil Hall [b], Tomoyoshi Nozaki [c,d,*]

[a] *Department of Parasitology, National Institute of Infectious Diseases, Shinjuku-ku, Tokyo 162-8640, Japan*
[b] *The Institute for Genomic Research, Rockville, MD 20850, USA*
[c] *Department of Parasitology, Gunma University Graduate School of Medicine, 3-39-22 Showa-machi, Maebashi, Gunma 371-8511, Japan*
[d] *Precursory Research for Embryonic Science and Technology, Japan Science and Technology Agency, 2-20-5 Akebono-cho, Tachikawa, Tokyo 190-0012, Japan*

Received 31 January 2005; received in revised form 31 January 2005; accepted 16 February 2005
Available online 7 April 2005

Abstract

Rab proteins are ubiquitous small GTP-binding proteins that form a highly conserved family and regulate vesicular trafficking. Recent completion of the genome of the enteric protozoan parasite *Entamoeba histolytica* enabled us to identify an extremely large number (>90) of putative Rab genes. Multiple alignment and phylogenic analysis of amebic, human, and yeast Rab showed that only 22 amebic Rab proteins including *Eh*Rab1, *Eh*Rab2, *Eh*Rab5, *Eh*Rab7, *Eh*Rab8, *Eh*Rab11, and *Eh*Rab21 showed significant similarity to Rab from other organisms. The 69 remaining amebic Rab proteins showed only moderate similarity (<40% identity) to Rab proteins from other organisms. Approximately one-third of Rab proteins including Rab7, Rab11, and RabC form 15 subfamilies, which contain up to nine isoforms. Approximately 70% of amebic Rab genes contain single or multiple introns, and this proportion is significantly higher than that of common genes in this organism. Twenty-five Rabs possess an atypical carboxyl terminus such as CXXX, XCXX, XXCX, XXXC, and no cysteine. We propose annotation of amebic Rab genes and discuss biological significance of this extraordinary diversity of *Eh*Rab proteins in this organism.

Index Descriptors and Abbreviations: DNA, deoxyribonucleic acid; *Eh*Rab, *Entamoeba histolytica* Rab; GTP, guanosine 5′-triphosphate

Keywords: *Entamoeba histolytica*; Membrane traffic; Phylogeny; Rab GTPase

1. Introduction

Small GTP-binding proteins are ubiquitous molecular switches involved in a variety of important cellular processes including cell proliferation, cytoskeletal assembly, and intracellular membrane trafficking in all eukaryotes. This superfamily is classified into five families: Ras, Rho/Rac, Rab, Sar/Arf, and Ran families based on its primary sequences (Bourne et al., 1990; Takai et al., 2001). Rab GTPases constitute the largest group of this superfamily and known as essential regulators of vesicular transport pathways (Novick and Zerial, 1997). In general, but not necessarily always, the complexity of Rab genes correlate with multicellularity of organisms. The higher the number of cells consisting of an organism, the higher the number of Rab genes encoded in its genome is. For example, unicellular yeast *Saccharomyces pombe*, *Saccharomyces cerevisiae*, and a nematode *Caenorhabditis elegans*, a fruit fly *Drosophila melanogaster*, or human *Homo sapiens*, which consists of one, ~10^3, 10^9, or 10^{13} cells, have 7, 11, 29, 29, or 60 Rab genes, respectively (Pereira-Leal and Seabra, 2001). In multicellular organisms, several Rab proteins are expressed in a highly coordinated (i.e., tissue-, organ- or developmental

☆ Nucleotide sequence data reported in this paper have been submitted to the DDBJ/EBI/GenBank Data Bank with Accession Nos. AB197055 to AB197121.

* Corresponding author. Fax: +81 27 220 8025.
E-mail address: nozaki@med.gunma-u.ac.jp (T. Nozaki).

0014-4894/$ - see front matter © 2005 Elsevier Inc. All rights reserved.
doi:10.1016/j.exppara.2005.02.021

stage-specific) fashion (Seabra et al., 2002; Zerial and McBride, 2001).

The enteric protozoan parasite *E. histolytica* is a etiological agent of amoebiasis, causing an estimated 50 million cases of amebic colitis, dysentery, and extraintestinal abscesses (Petri, 2002) and 40,000–100,000 deaths annually (WHO/PAHO/UNESCO, 1997). The size of the recently completed genome of *E. histolytica* (Loftus et al., 2005) is 20 Mb, which is about 1.6 times of *S. cerevisiae* and one fifth of *C. elegans*. We and other groups have previously reported 16 *Eh*Rab genes, identified by cDNA isolation using degenerate PCR primers and homology-based search (Juarez et al., 2001; Rodriguez et al., 2000; Saito-Nakano et al., 2001, 2004; Temesvari et al., 1999). However, the complexity of Rab genes in *E. histolytica* remains totally unknown. In this paper, we describe identification of additional 75 *Eh*Rab genes by thorough search of the latest genome database. To our knowledge, this is the first demonstration of a uni- or multi-cellular organism possessing more than 90 Rab genes. Based on our analysis, we propose annotation of amebic Rab genes.

2. Methods

Nucleotide and protein sequences of human and yeast Rab were retrieved from GenBank. For accession numbers of these proteins, see (Pereira-Leal and Seabra, 2001). To obtain a maximum number of Rab genes from *E. histolytica*, we first searched for putative homologues of all yeast and human small GTPases including Rab, Ras/Rap, Rho/Rac, Arf/Sar, and Ran against a translated protein subset of the *E. histolytica* genome database (http://www.tigr.org/tdb/e2k1/eha1/) using BLASTP algorism. Additionally, we used *E. histolytica*-specific members of Rab, Ras, and Rho/Rac, e.g., RabA (Temesvari et al., 1999), Ras4 (Kumagai et al., 2004), and RacD (Lohia and Samuelson, 1996), as an inquiry. Altogether, we obtained 146 possible small GTPases. All the possible *Entamoeba* Rab protein sequences were re-examined with BLASTP analysis using individual amebic protein as an inquiry sequence against the human database at National Center of Biotechnology Information (NCBI). Among 146 possible small GTPases, 55 sequences were tentatively assigned as Sar/Arf, Ras/Rap, Rho/Rac, or Ran, as they showed highest identities to these small GTPase subfamilies from human. One should be cautious that due to the method we used to retrieve sequences, it is possible additional small GTPases may exist in *E. histolytica*. The 91 remaining small GTPases were individually verified for the presence of conserved GTP-binding consensus sequences (GDXX-VGKT, DTAGQE, and GNKXD) and additional five conserved regions that are specific only to Rab family (IGVDF, KLQIW, RFRSIT, YYRGA, and LVYDIT) (Pereira-Leal and Seabra, 2000) by manual inspections. In the present study, these 91 putative Rab are further analyzed. Highly conserved domains stretching from the first to the third GTP-binding consensus regions of 91 *E. histolytica*, 7 *S. cerevisiae*, and 35 human Rab proteins were aligned using the CLUSTAL W program version 1.81 (Thompson et al., 1994) with default parameters. After alignments were manually corrected and non-aligned gaps were removed, 110 unambiguously aligned sites were selected and used for phylogenetic analysis by the neighbor-joining method (Saitou and Nei, 1987). Phylogenetic trees were drawn using the TreeView software (http://taxonomy.zoology.gla.ac.uk/rod/rod.html).

3. Results and discussion

3.1. Identification and annotation of 91 EhRab proteins

We identified 91 putative Rab proteins in the *E. histolytica* genome database (Loftus et al., 2005). They included 16 previously reported Rab proteins consisting of putative amebic homologues of human Rab1, Rab2, Rab5, Rab7, Rab8, Rab11, and Rab proteins that showed limited homology (<40% identity) to Rab from other organisms and were annotated as *Eh*RabA to *Eh*RabI (Juarez et al., 2001; Rodriguez et al., 2000; Saito-Nakano et al., 2001, 2004; Temesvari et al., 1999). Twenty-two of 91 amebic Rab showed >40% identity to human Rab1/yeast Ypt1p, human Rab2/Rab4/Rab14, Rab5/Ypt5p, Rab7/Ypt7p, Rab8/Sec4p, Rab11/Ypt31p, or human Rab21 and were considered to be their amebic homologues. We accordingly designated them as *Eh*Rab1A-1B, *Eh*Rab2A-2C, *Eh*Rab5, *Eh*Rab7A-7I, *Eh*Rab8-8B, *Eh*Rab11A-11D, and *Eh*Rab21, where the alphabet after the number represents an individual isotype, in case where their overall identity to human or yeast homologues was >40% (Tables 2–6). Among the remaining 69 *E. histolytica*-specific Rab proteins, 30 Rab proteins showed >40% mutual identity to one or more of these 30 amebic Rab and clustered in nine subgroups designated as *Eh*RabC, *Eh*RabD, *Eh*RabF, *Eh*RabI, EhRabK, *Eh*RabL, *Eh*RabM, *Eh*RabN, and *Eh*RabP subfamilies (Tables 7–10). The residual 39 Rab, including previously reported 3 *Eh*Rab, i.e., *Eh*RabA, *Eh*RabB, and *Eh*RabH, represent novel and solitary amebic Rab proteins showing low homology to Rab from human, yeast, and to other members of the amebic Rab. Accordingly we designated these newly identified solitary Rab as *Eh*RabX1 to *Eh*RabX36 (Fig. 1 and Table 1).

3.2. EhRab proteins showing significant homology to human or yeast counterparts

Entamoeba histolytica possesses at least nine isotypes of Rab7 (*Eh*Rab7A–*Eh*Rab7I, Fig. 1, Table 5), which has

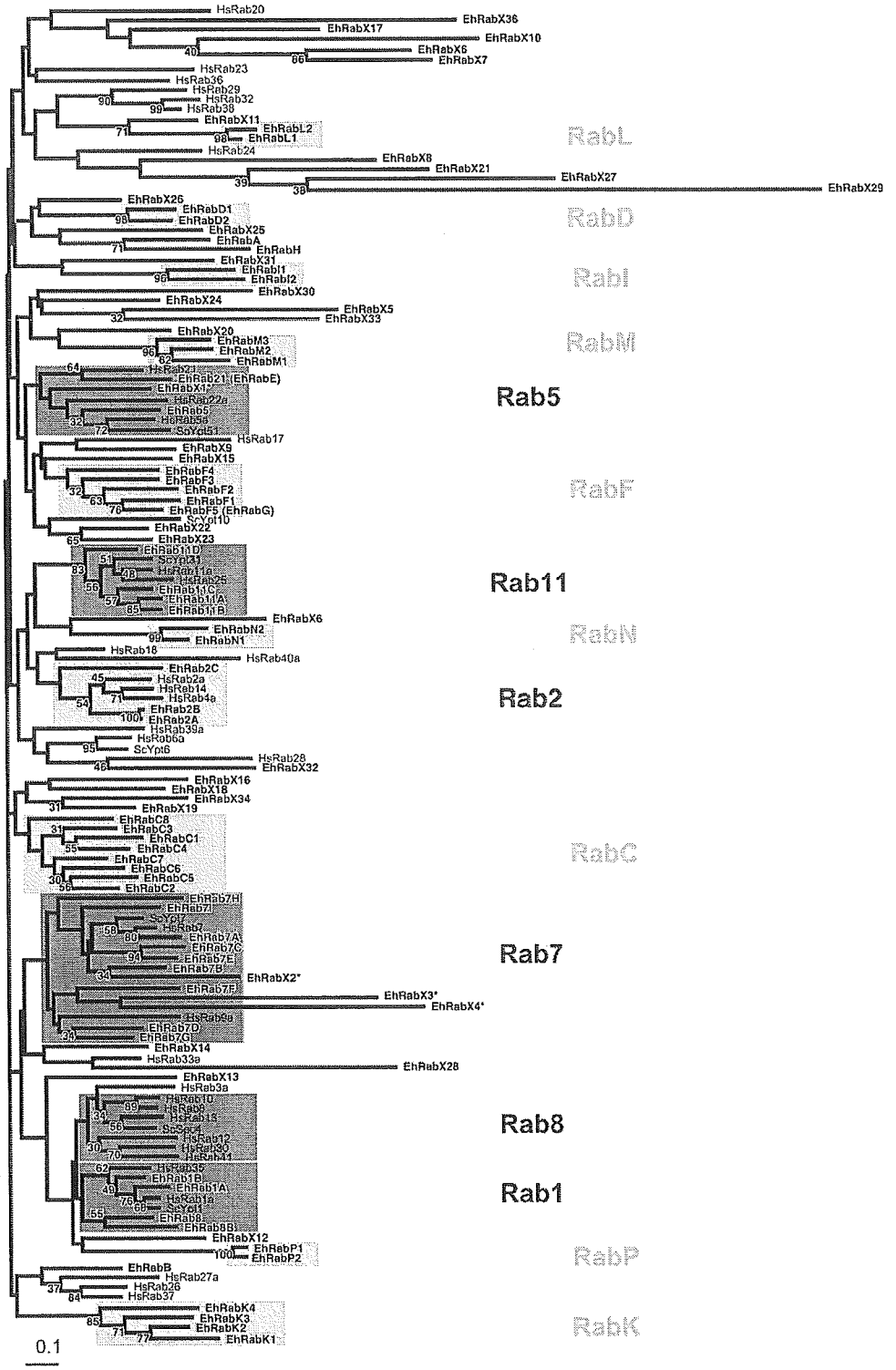

Fig. 1. A phylogenic tree of Rab proteins from *E. histolytica*, human, and yeast. The numbers on the nodes represent the bootstrap proportions (%) of 1000 pseudo samples; only bootstrap proportions >30% are shown. *E. histolytica* Rab proteins are indicated in bold. Tentative subfamilies that revealed significant homology (>40% identity) to human or yeast counterpart are shaded by dark boxes, while *Entamoeba*-specific subfamilies are highlighted by light boxes. Asterisks indicate Rab proteins that were not considered as isotypes of the subfamily based on <40% identity to other members of the subfamily. The scale bar indicates 0.1 substitutions at each amino acid position.

Table 1
A list of 91 *Eh* Rab proteins and their features of nucleotide and amino acid sequences

Name	Previous name	Accession No.	No. of intron	Missing regions	C-terminal peptides	References
Eh Rab1A	*Eh* Rab1	AB054578	1		CXXX	3,6
Eh Rab1B		AB197055	3		XXCC	
Eh Rab2A		AB197071	1		—	
Eh Rab2B		AB197072	1		—	
Eh Rab2C		AB197073	1		—	
Eh Rab5		AB054582	1		XXCC	5
Eh Rab7A	*Eh* Rab7	AB054583	—		XCXC	1,5,6
Eh Rab7B		AB186363	1		XCXC	6
Eh Rab7C		AB186364	1		XXCC	6
Eh Rab7D		AB186365	—		XXCC	6
Eh Rab7E		AB186366	1		XXCC	6
Eh Rab7F		AB186367	1		XXCC	
Eh Rab7G		AB186368	—		XXCC	
Eh Rab7H		AB186369	1		XXCC	
Eh Rab7I		AB197056	3		XXCC	
Eh Rab8		AF363067	1		XXCC	4
Eh Rab8B		AB197057	1		XXCC	
Eh Rab11A	*Eh* Rab11	AB186370	1		XXCC	1
Eh Rab11B		AB054587	—		XXCC	3
Eh Rab11C		AB054588	—		XXCC	3
Eh Rab11D		AB197058	1		XCXC	
Eh Rab21	*Eh* RabE	AB054581	1	switch I	XXCC	3
Eh RabA		AF030184	2		XCXC	1
Eh RabB		AF127375	—		XXCC	2
Eh RabC1	*Eh* RabC	AB054579	—		XXCC	3,6
Eh RabC2		AB186371	—		XXCC	
Eh RabC3		AB197059	—		XXCC	
Eh RabC4		AB197060	—		XXCC	
Eh RabC5		AB197061	1		XXCC	
Eh RabC6		AB197062	2		XXCC	
Eh RabC7		AB197063	2		XXCC	
Eh RabC8		AB197064	1		XXCC	
Eh RabD1	*Eh* RabD	AB054580	—		XXCC	3
Eh RabD2		AB197065	—		XXCC	
Eh RabF1	*Eh* RabF	AB054584	1		CXXX	3
Eh RabF2		AB197068	3		XXCC	
Eh RabF3		AB197067	2		XXCC	
Eh RabF4		AB197066	1		XXCC	
Eh RabF5	*Eh* RabG	AB054585	1		XXXC	3
Eh RabH		AB054586	—	switch II	XCXC	3
Eh RabI1	*Eh* RabI	AB054589	2	switch I, II	XCXC	3
Eh RabI2		AB197069	1		XCXC	
Eh RabK1		AB197077	—		XXCC	
Eh RabK2		AB197079	1		XXCC	
Eh RabK3		AB197078	3		XXCC	
Eh RabK4		AB197120	1	switch I	XXCC	
Eh RabL1		AB197081	1		XCCX	
Eh RabL2		AB197080	1		XCCX	
Eh RabM1		AB197083	4	box 2, 3	XXCC	
Eh RabM2		AB197084	—		XXCC	
Eh RabM3		AB197082	2		XXCC	
Eh RabN1		AB197085	2		XCXX	
Eh RabN2		AB197086	1		XXXC	
Eh RabP1		AB197087	—		CXXX	
Eh RabP2		AB197088	1		CXXX	
Eh RabX1		AB197070	3		XXCC	
Eh RabX2		AB197074	—		XXCC	
Eh RabX3		AB197075	3	switch I, II	—	
Eh RabX4		AB197076	—	switch I	XXCX	
Eh RabX5		AB197089	1	switch II	XXXC	
Eh RabX6		AB197090	1	switch II	CXXX	
Eh RabX7		AB197091	1	switch I, II	CXXX	

(*continued on next page*)

Table 1 (*continued*)

Name	Previous name	Accession No.	No. of intron	Missing regions	C-terminal peptides	References
Eh RabX8		AB197092	—	switch I, II, box 2, 3	CCXX	
Eh RabX9		AB197093	3		XXCC	
Eh RabX10		AB197094		switch I, II	CCXXX	
Eh RabX11		AB197095	2		XXCC	6
Eh RabX12		AB197096	2		XXCC	
Eh RabX13		AB197097	1		XXCC	
Eh RabX14		AB197098	1		XXCC	
Eh RabX15		AB197099	1		XXCC	
Eh RabX16		AB197100	—		XXCC	
Eh RabX17		AB197101	—	switch I	CXXX	
Eh RabX18		AB197102	1		CXXX	
Eh RabX19		AB197103	2		XXCC	
Eh RabX20		AB197104	—		XXCC	
Eh RabX21		AB197105	1	switch II	CXXXXX	
Eh RabX22		AB197106	2		XXCC	
Eh RabX23		AB197107	2		XXCC	
Eh RabX24		AB197108	1	switch I	XXCC	
Eh RabX25		AB197109	—		XXCC	
Eh RabX26		AB197110	1		XXCC	
Eh RabX27		AB197111	1	box 2, 3	CXXX	
Eh RabX28		AB197112	—	box 1, 3	CXXX	
Eh RabX29		AB197113	1	switch I, II, box 2	CXXX	
Eh RabX30		AB197114	1		CXXX	
Eh RabX31		AB197115	1		XXCC	
Eh RabX32		AB197116	2	box 2	CXXXXX	
Eh RabX33		AB197117	2	switch I	CCXXX	
Eh RabX34		AB197118	1		CXXX	
Eh RabX35		AB197119	—		XXCC	
Eh RabX36		AB197121	—	switch I	—	

Reference 1, Temesvari et al. (1999); 2, Rodriguez et al. (2000); 3, Saito-Nakano et al. (2001); 4, Juarez et al. (2001); 5, Saito-Nakano et al. (2004); and 6, Okada et al. (2005).

no precedent in unicellular eukaryotes as well as fly, worm, and mammals (Pereira-Leal and Seabra, 2001). In human, Rab7 and related Rab9 were shown to be involved in late endocytic trafficking (Rodman and Wandinger-Ness, 2000). We previously showed in *E. histolytica* Rab7A plays a role in the biogenesis of the unique organelle to this organism ("prephagosomal vacuole") and also in the processing, storage, and transport to phagosomes of digestive proteins (Saito-Nakano et al., 2004). It was also shown that *Eh*Rab7A was concentrated in endosome-enriched fraction (Temesvari et al., 1999). At least five *Eh*Rab7 isotypes (*Eh*Rab7A-7E) were identified by proteomic analysis of latex bead-containing phagosomes, suggesting the involvement of multiple Rab7 isotypes in phagosome biogenesis (Okada et al., 2005). Although three other Rab proteins, *Eh*RabX2-X4 were clustered in a same clade in the phylogenetic reconstruction, they were not considered as Rab7 isotypes based on the fact that they showed <40% identities to any Rab7 isotypes from *E. histolytica*, yeast, or human (Table 5).

In general Rab11/Ypt31p function in the recycling of membrane proteins on recycling endosomes (Rodman and Wandinger-Ness, 2000) and form a cluster together with human Rab25 (Pereira-Leal and Seabra, 2001), which showed similar subcellular localization to Rab11 (Casanova et al., 1999). *E. histolytica* possesses four

Table 2
Amino acid identities among Rab1 and closely related homologues from *E. histolytica*, human, and yeast

	EhRab1A	EhRab1B	HsRab1a	ScYpt1	HsRab35	EhRab8	EhRab8B	HsRab8a	ScSec4
EhRab1A	100	56	60	55	47	47	40	46	45
EhRab1B		100	58	56	53	49	49	54	49
HsRab1a			100	71	54	51	42	52	50
ScYpt1				100	49	51	42	48	47
HsRab35					100	43	41	45	42
EhRab8						100	54	50	47
EhRab8B							100	42	42
HsRab8a								100	50
ScSec4									100

Eh, *E. histolytica*; Hs, *Homo sapiens*; and Sc, *Saccharomyces cerevisiae*.

Table 3
Amino acid identities among Rab2 and closely related homologues from *E. histolytica* and human

	EhRab2A	EhRab2B	EhRab2C	HsRab2a	HsRab14	HsRab4
EhRab2A	100	89	46	51	46	40
EhRab2B		100	45	51	46	42
EhRab2C			100	37	38	35
HsRab2a				100	56	51
HsRab14					100	59
HsRab4						100

Values less than 40% are shown in reverse.

Rab11 homologues (*Eh*Rab11A-11D) including *Eh*Rab11A, which was proposed to play a role during encystation (McGugan and Temesvari, 2003) and previously identified *Eh*Rab11B and *Eh*Rab11C (Saito-Nakano et al., 2001; Temesvari et al., 1999) (Table 6).

Despite significant similarity to human and yeast homologues (51 and 43% identity, respectively), which are localized to endosomes (Zerial and McBride, 2001), Rab5 was shown to be excluded from endocytic pathway in *E. histolytica* (Saito-Nakano et al., 2004). We also previously showed that *Eh*Rab5 is involved, together with *Eh*Rab7A, in the initial phase of biogenesis of prephagosomal vacuoles, and is essential for efficient phagocytosis (Saito-Nakano et al., 2004). In contrast to yeast, where three isotypes with apparently redundant function exist, no additional *Eh*Rab5 isotype is present in this organism (Fig. 1). Previously reported *Eh*RabE (Saito-Nakano et al., 2001) showed 47% identity to human Rab21, which localizes to early endosomes like Rab5 and Rab22 (Simpson et al., 2004; Table 4). We redesignated *Eh*RabE as *Eh*Rab21 based on the criteria described above.

We identified four putative Rab1/Rab8 homologues (Table 2), which include previously described *Eh*Rab1 (AB054578), showing 60% identity to human Rab1a, and *Eh*Rab8 (AF363067), which shows 42% identity to human Rab8a (Juarez et al., 2001; Saito-Nakano et al., 2001) and was proposed to be involved in the targeting of vesicles to plasma membrane (Juarez et al., 2001). We designated the other two Rab proteins as *Eh*Rab1B and *Eh*Rab8B as the former shows highest similarity to human Rab1a and the latter shows highest identity to *Eh*Rab8.

We identified three putative Rab2/Rab4/Rab14 homologues (Table 3). Although human Rab2, Rab4, and Rab14 belong to one subfamily (Pereira-Leal and Seabra, 2001), they reveal distinct localizations and functions Rab2, Rab4, or Rab14 is localized in the ER-to-Golgi, early endosomes, or Golgi-to-endosomes (Junutula et al., 2004; Mohrmann et al., 2002; Tisdale, 1999).

3.3. EhRab proteins with no obvious homologues from other organisms

Sixty-nine of 91 *Eh*Rab proteins showed <40% identity to human and yeast Rab, are presumed to be unique to this organism. Thirty of these ameba-specific Rabs also form nine subfamilies (Tables 7–10) and designated as e.g., *Eh*RabC3, where the alphabet represents a subfamily and the number after the alphabet represents an individual isotype. The largest *E. histolytica*-specific group (only after *Eh*Rab7 subfamily described above), *Eh*RabC subfamily, consists of eight isotypes, *Eh*RabC1-C8 (Table 7). *Eh*RabC1-C3 were identified from isolated phagosomes (C1, Okada et al., 2005; C2 and C3, Okada and Nozaki, unpublished), suggesting that these three members of *Eh*RabC subfamily are involved in phagosome biogenesis. Four isotypes of *Eh*RabF (*Eh*RabF1-F4) as well as *Eh*RabG were grouped in the same subfamily, *Eh*RabG was renamed as *Eh*RabF5 (Tables 1 and 8). Other Rab proteins were also grouped in subfamilies: *Eh*RabD1-D2, *Eh*RabI1-I2,, *Eh*RabK1-K4, *Eh*RabL1-L2, *Eh*RabM1-M3, *Eh*RabN1-N2, and *Eh*RabP1-P2 (Tables 9 and 10).

Table 4
Amino acid identities among Rab5 and closely related homologues from *E. histolytica*, human, and yeast

	EhRab5	HsRab5a	ScYpt51	HsRab22a	EhRabX1	HsRab21	EhRab21/E
EhRab5	100	51	43	44	30	40	36
HsRab5a		100	48	47	36	38	29
ScYpt51			100	39	36	37	32
HsRab22a				100	37	39	30
EhRabX1					100	33	30
HsRab21						100	47
EhRab21/E							100

Values less than 40% are shown in reverse.

Table 5
Amino acid identities among Rab7 and closely related homologues from *E. histolytica*, human, and yeast

	EhRab7A	EhRab7B	EhRab7C	EhRab7D	EhRab7E	EhRab7F	EhRab7G	EhRab7H	EhRab7I	EhRabX2	EhRabX3	EhRabX4	HsRab7a	HsRab9	ScYpt7	EhRab5	HsRab5a
EhRab7A	100	45	44	39	45	41	36	32	35	37	16	21	56	46	54	27	29
EhRab7B		100	46	49	49	38	36	35	46	39	15	25	49	42	46	27	29
EhRab7C			100	46	64	42	43	40	42	36	15	18	51	46	46	32	28
EhRab7D				100	46	38	51	40	36	36	35	12	47	45	42	34	29
EhRab7E					100	40	43	33	39	35	15	19	46	42	46	29	30
EhRab7F						100	36	33	35	30	10	23	42	36	45	30	30
EhRab7G							100	37	38	31	18	21	40	40	37	31	31
EhRab7H								100	36	25	24	15	35	32	32	38	28
EhRab7I									100	32	15	18	41	33	37	35	33
EhRabX2										100	11	19	38	33	36	26	21
EhRabX3											100	18	18	17	22	22	18
EhRabX4												100	22	19	22	21	15
HsRab7a													100	48	62	34	34
HsRab9														100	47	31	27
ScYpt7															100	37	28
EhRab5																100	51
HsRab5a																	100

Values less than 40% are shown in reverse. EhRab5 and HsRab5a are included as control.

3.4. Peculiarity of nucleotide and protein sequences

Approximately 70% (64) of amebic *Rab* genes contained introns, and 23% (22) of amebic *Rab* genes contained 2–4 introns (Table 1). Considering that among 9938 predicted open reading frames of the entire *Entamoeba* genome only 25.2% of genes have introns and 6% of these genes contained multiple introns (Loftus et al., 2005), and that the average size of amebic *Rab* genes is 702 bp, which is shorter than that of all genes (1173 bp), indicating that amebic *Rab* genes are extremely intron rich.

Rab GTPases typically have three GTP-binding consensus, Rab-specific effector (also called "Switch I"), and α2 helix ("Switch II") regions (Pereira-Leal and Seabra, 2000). The "Switch I and II" regions are located on the surface of the molecule as demonstrated in structural studies, and crucial for the interaction with regulatory proteins (effectors) such as guanine nucleotide exchange factors and GTPase-activating proteins (Stenmark and Olkkonen, 2001). While the GTP-binding consensus regions (boxes 1–3) are conserved in the small GTPase superfamily, the "Switch I and II" regions are unique to Rab GTPases. About 20% of amebic Rab proteins lack one or more of these functional regions (Table 1). We have a line of evidence supporting that these *Eh*Rab genes are functional GTPase. First, *Eh*Rab21, *Eh*RabH, and *Eh*RabII, which lack one or both of Switch I and II regions, are expressed as mRNA in the axenic trophozoites, which excludes a possibility of pseudogenes (Saito-Nakano et al., 2001). In addition, *Eh*Ras4, which lacks the Switch I region and one of the GTP-binding consensus regions, showed a GTP-binding activity in vitro (Kumagai et al., 2004). These data suggest that amebic Rab that lack these conserved regions are likely functional, and that it is not easy, in general, to predict functionality of these important regions and domains of the amebic small GTPases by the primary protein sequences.

It has been well established that Rab proteins are lipid-modified at the carboxyl terminus by isoprenylation with Rab geranylgeranyl transferase (geranylgeranyl transferase II) (Takai et al., 2001). Prenylation motifs located at the carboxyl terminus of Rab generally consist of two cysteine residues such as XXCC, XCCX, CCXX, and XCXC (Takai et al., 2001). While the majority of amebic Rab proteins contain two cysteine residues at the carboxyl terminus, about 13% (13) possess a single cysteine, such as CXXX, which was often found in Ras and Rho/Rac subfamilies (Table 1). Five amebic Rab proteins totally lack cysteine at the carboxyl terminus. It has been reported that a number of human Rab also lack the typical carboxyl termini; 8 Rab possess no cysteine and other 8 Rab contain a single cysteine (Pereira-Leal and Seabra, 2001). Interestingly, seven amebic Rab proteins contain novel types of carboxyl termini containing a single cysteine: XCXX, XXCX, XXXC or

Table 6
Amino acid identities among Rab11 and closely related homologues from *E. histolytica*, human, and yeast

	EhRab11A	EhRab11B	EhRab11C	EhRab11D	HsRab11a	ScYpt31	HsRab25
EhRab11A	100	63	58	55	57	42	51
EhRab11B		100	56	58	54	43	48
EhRab11C			100	51	51	42	42
EhRab11D				100	51	40	42
HsRab11a					100	44	57
ScYpt31						100	42
HsRab25							100

Table 7
Amino acid identities among RabC isotypes from *E. histolytica*

	EhRabC1	EhRabC2	EhRabC3	EhRabC4	EhRabC5	EhRabC6	EhRabC7	EhRabC8
EhRabC1	100	44	55	49	41	42	41	37
EhRabC2		100	46	41	57	53	48	48
EhRabC3			100	49	44	45	40	34
EhRabC4				100	40	40	41	39
EhRabC5					100	49	44	43
EhRabC6						100	52	50
EhRabC7							100	49
EhRabC8								100

Values less than 40% are shown in reverse.

Table 8
Amino acid identities among RabF and related homologues from *E. histolytica* and human

	EhRabF	EhRabF5/G	EhRabF2	EhRabF3	EhRabF4	EhRabX21	HsRab17	EhRabX15
EhRabF	100	59	44	44	40	33	33	31
EhRabF5/G		100	43	45	41	38	31	33
EhRabF2			100	45	48	32	29	32
EhRabF3				100	47	38	32	27
EhRabF4					100	39	35	35
EhRabX21						100	29	28
HsRab17							100	26
EhRabX15								100

Values less than 40% are shown in reverse.

Table 9
Amino acid identities among RabK isotypes in *E. histolytica*

	EhRabK1	EhRabK2	EhRabK3	EhRabK4
EhRabK1	100	60	47	39
EhRabK2		100	45	41
EhRabK3			100	37
EhRabK4				100

Values less than 40% are shown in reverse.

Table 10
Pairwise amino acid identities between isotypes that belong to RabD, RabI, RabL, RabM, RabN, and RabP subfamilies

Subfamilies	
EhRabD1:EhRabD2	60
EhRabI1:EhRabI2	52
EhRabL1:EhRabL2	62
EhRabM1:EhRabM2	56
EhRabM2:EhRabM3	65
EhRabM1:EhRabM3	54
EhRabN1:EhRabN2	75
EhRabP1:EhRabP2	85

CXXXXX, which have not been reported in human (Pereira-Leal and Seabra, 2001).

Finally, the diversity and complexity of Rab proteins we report here may reflect the vigorous dynamism of the membrane transport and the committed reliance on Rab proteins in the determination of specificity of vesicular trafficking in this unicellular protozoan parasite. In addition, the presence of unique structural exceptions including lack of conserved functional boxes and domains, and non-conventional carboxyl terminus found in some Rab proteins may suggest that novel Rab modifications and functions exist in this organism. Further analysis of such peculiarities may help in the elucidation of functional constrains during evolution and the ameba-specific biological mechanisms, which are likely associated with its unique virulent competence.

Acknowledgments

We are grateful to Tetsuo Hashimoto, Tsukuba University, for many helpful comments and discussions. We thank Mami Okada, Mai Nudejima, and Yumiko Tsukamoto for their technical assistance. This work was supported in part by a grant for Precursory Research for Embryonic Science and Technology (PRESTO), Japan Science and Technology Agency, Grant-in-Aid for Scientific Research from the Ministry of Education, Culture, Sports, Science and Technology of Japan to Y.S-N. (15790219) and T.N. (16017307, 16044250, and 15590378), and a grant for the Project to Promote Development of Anti-AIDS Pharmaceuticals from the Japan Health Sciences Foundation to T.N.

References

Bourne, H.R., Sanders, D.A., McCormick, F., 1990. The GTPase superfamily: a conserved switch for diverse cell functions. Nature 348, 125–132.

Casanova, J.E., Wang, X., Kumar, R., Bhartur, S.G., Navarre, J., Woodrum, J.E., Altschuler, Y., Ray, G.S., Goldenring, J.R., 1999. Association of Rab25 and Rab11a with the apical recycling system of polarized Madin–Darby canine kidney cells. Molecular Biology of the Cell 10, 47–61.

Juarez, P., Sanchez-Lopez, R., Stock, R.P., Olvera, A., Ramos, M.A., Alagon, A., 2001. Characterization of the *Eh*Rab8 gene, a marker of the late stages of the secretory pathway of *Entamoeba histolytica*. Molecular and Biochemical Parasitology 116, 223–228.

Junutula, J.R., De Maziere, A.M., Peden, A.A., Ervin, K.E., Advani, R.J., van Dijk, S.M., Klumperman, J., Scheller, R.H., 2004. Rab14 is involved in membrane trafficking between the Golgi complex and endosomes. Molecular Biology of the Cell 15, 2218–2229.

Kumagai, M., Makioka, A., Takeuchi, T., Nozaki, T., 2004. Molecular cloning and characterization of a protein farnesyltransferase from the enteric protozoan parasite *Entamoeba histolytica*. Journal of Biological Chemistry 279, 2316–2323.

Loftus, B., Anderson, I., Davies, R., Alismark, U.C.M., Samuelson, J., Amedeo, P., Roncaglia, P., Berriman, M., Hirt, R.P., Mann, B.J. Nozaki, T., Suh, B., Pop, M., Duchene, M., Ackers, J., Tannich, E., Leippe, M., Hofer, M., Bruchhaus, I., Willhoeft, U., Bhattacharya, A., Chillingworth, T., Churcher, C., Hance, Z., Harris, B., Harris, D., Jagels, K., Moule, S., Mungall, K., Ormond, D., Squares, R., Whitehead, S., Guillén, N. Gilchrist, C., Stroup, S.E., Bhattacharya, S., Lohia, A., Foster, P.G., Sicheritz-Ponten, T., Weber, C., Singh, U., Mukherjee, C., Petri, Jr., W.A., Clark, C.G., Embley, T.M., Barrell, B., Fraser, C.M., Hall, N., 2005. The genome of the protist parasite *Entamoeba histolytica*. Nature 433, 865–868.

Lohia, A., Samuelson, J., 1996. Heterogeneity of *Entamoeba histolytica* rac genes encoding p21rac homologues. Gene 173, 205–208.

McGugan, G.C.J., Temesvari, L.A., 2003. Characterization of a Rab11-like GTPase, *Eh*Rab11, of *Entamoeba histolytica*. Molecular and Biochemical Parasitology 129, 137–146.

Mohrmann, K., Gerez, L., Oorschot, V., Klumperman, J., van der Sluijs, P., 2002. Rab4 function in membrane recycling from early endosomes depends on a membrane to cytoplasm cycle. Journal of Biological Chemistry 277, 32029–32035.

Novick, P., Zerial, M., 1997. The diversity of Rab proteins in vesicle transport. Current Opinion in Cell Biology 9, 496–504.

Okada, M., Huston, C.D., Mann, B.J., Petri, W.A.J., Kita, K., Nozaki, T., 2005. Proteomic analysis of phagocytosis in the enteric protozoan parasite *Entamoeba histolytica*. Eukaryotic Cell, in press.

Pereira-Leal, J.B., Seabra, M.C., 2000. The mammalian Rab family of small GTPases: definition of family and subfamily sequence motifs suggests a mechanism for functional specificity in the Ras superfamily. Journal of Molecular Biology 301, 1077–1087.

Pereira-Leal, J.B., Seabra, M.C., 2001. Evolution of the Rab family of small GTP-binding proteins. Journal of Molecular Biology 313, 889–901.

Petri Jr., W.A., 2002. Pathogenesis of amebiasis. Current Opinion in Microbiology 5, 443–447.

Rodman, J.S., Wandinger-Ness, A., 2000. Rab GTPases coordinate endocytosis. Journal of Cell Science 113, 183–192.

Rodriguez, M.A., Garcia-Perez, R.M., Garcia-Rivera, G., Lopez-Reyes, I., Mendoza, L., Ortiz-Navarrete, V., Orozco, E., 2000. An *Entamoeba histolytica* rab-like encoding gene and protein: function and cellular location. Molecular and Biochemical Parasitology 108, 199–206.

Saitou, N., Nei, M., 1987. The neighbour-joining method: a new method to reconstruct phylogenetic trees. Molecular Biology of Evolution 4, 406–425.

Saito-Nakano, Y., Nakazawa, M., Shigeta, Y., Takeuchi, T., Nozaki, T., 2001. Identification and characterization of genes encoding novel Rab proteins from *Entamoeba histolytica*. Molecular and Biochemical Parasitology 116, 219–222.

Saito-Nakano, Y., Yasuda, T., Nakada-Tsukui, K., Leippe, M., Nozaki, T., 2004. Rab5-associated vacuoles play a unique role in phagocytosis of the enteric protozoan parasite *Entamoeba histolytica*. Journal of Biological Chemistry 279, 49497–49507.

Seabra, M.C., Mules, E.H., Hume, A.N., 2002. Rab GTPases, intracellular traffic and disease. Trends in Molecular Medicine 8, 23–30.

Simpson, J.C., Griffiths, G., Wessling-Resnick, M., Fransen, J.A., Bennett, H., Jones, A.T., 2004. A role for the small GTPase Rab21 in the early endocytic pathway. Journal of Cell Science 117, 6297–6311.

Stenmark, H., Olkkonen, V.M., 2001. The Rab GTPase family. Genome Biology 2, REVIEWS3007.1-3007.7.

Takai, Y., Sasaki, T., Matozaki, T., 2001. Small GTP-binding proteins. Physiological Reviews 81, 153–208.

Temesvari, L.A., Harris, E.N., Stanley, S.L.J, Cardelli, J.A., 1999. Early and late endosomal compartments of *Entamoeba histolytica* are enriched in cysteine proteases, acid phosphatase and several Ras-related Rab GTPases. Molecular and Biochemical Parasitology 103, 225–241.

Thompson, J.D., Higgins, D.G., Gibson, T.J., 1994. CLUSTAL W: improving the. sensitivity of progressive multiple sequence alignment through sequence weighting, positive-specific gap penalties and weight matrix choice. Nucleic Acids Research 22, 4673–4680.

Tisdale, E.J., 1999. A Rab2 mutant with impaired GTPase activity stimulates vesicle formation from pre-Golgi intermediates. Molecular Biology of the Cell 10, 1837–1849.

WHO/PAHO/UNESCO. 1997. A consultation with experts on amebiasis. Epidemiological Bulletin 18, 13–14.

Zerial, M., McBride, H., 2001. Rab proteins as membrane organizers. Nature Reviews Molecular Cell Biology 2, 107–117.

Cell Motility and the Cytoskeleton 62:000–000 (2005)

Differences in Morphology of Phagosomes and Kinetics of Acidification and Degradation in Phagosomes Between the Pathogenic *Entamoeba histolytica* and the Nonpathogenic *Entamoeba dispar*

Biswa N. Mitra,[1] Tomoyoshi Yasuda,[2] Seiki Kobayashi,[3] Yumiko Saito-Nakano,[2] and Tomoyoshi Nozaki[1,4]*

[1]*Department of Parasitology, Gunma University Graduate School of Medicine, Maebashi, Gunma 371-851, Japan*
[2]*Department of Parasitology, National Institute of Infectious Diseases, Shinjuku-ku, Tokyo 162-8640, Japan*
[3]*Department of Parasitology, Keio University School of Medicine, Tokyo 160-8582, Japan*
[4]*The Precursory Research for Embryonic Science and Technology, Japan Science and Technology Agency, Tachikawa, Tokyo 190-0012, Japan*

Phagocytosis plays an important role in the pathogenicity of the intestinal protozoan parasite *Entamoeba histolytica*. We compared the morphology of phagosomes and the kinetics of phagosome maturation using conventional light and electron microscopy and live imaging with video microscopy between the virulent *E. histolytica* and the closely-related, but nonvirulent *E. dispar* species. Electron micrographs showed that axenically cultivated trophozoites of the two *Entamoeba* species revealed morphological differences in the number of bacteria contained in a single phagosome and the size of phagosomes. Video microscopy using pH-sensitive fluorescein isothiocynate-conjugated yeasts showed that phagosome acidification occurs within 2 min and persists for >12 h in both species. The acidity of phagosomes significantly differed between two species (4.58 ± 0.36 or 5.83 ± 0.38 in *E. histolytica* or *E. dispar*, respectively), which correlated well with the differences in the kinetics of degradation of promastigotes of GFP-expressing *Leishmania amazonensis*. The acidification of phagosomes was significantly inhibited by a myosin inhibitor, whereas it was only marginally inhibited by microtubules or actin inhibitors. A specific inhibitor of vacuolar ATPase, concanamycin A, interrupted both the acidification and degradation in phagosomes in both species, suggesting the ubiquitous role of vacuolar ATPase in the acidification and degradation in *Entamoeba*. In contrast, inhibitors against microtubules or cysteine proteases (CP) showed distinct effects on degradation in phagosomes between these two species. Although depolymerization of microtubules severely inhibited degradation in phagosomes of *E. histolytica*, it

Contract grant sponsor: The Ministry of Education, Culture, Sports, Science and Technology of Japan; Contract grant numbers: 15019120, 15590378, 16017307, and 16044250; Contract grant sponsors: The Ministry of Health, Labour, and Welfare and The Japan Health Sciences Foundation.

*Correspondence to: Tomoyoshi Nozaki, Department of Parasitology, Gunma University Graduate School of Medicine, 3-39-22 Showa-machi, Maebashi, Gunma 371-8511, Japan.
E-mail: nozaki@med.gunma-u.ac.jp

Received 28 March 2005; Accepted 21 June 2005

Published online in Wiley InterScience (www.interscience.wiley.com).
DOI: 10.1002/cm.20087

did not affect degradation in *E. dispar*. Similarly, the inhibition of CP significantly reduced degradation in phagosomes of *E. histolytica*, but not in *E. dispar*. These data suggest the presence of biochemical or functional differences in the involvement of microtubules and proteases in phagosome maturation and degradation between the two species. Cell Motil. Cytoskeleton 62:000–000, 2005.

Key words: phagocytosis; endocytosis; vacuolar ATPase; cysteine protease; amebiasis

INTRODUCTION

Phagocytosis is an essential process by which professional phagocytes (e.g., macrophages and neutrophils) engulf invading pathogens, apoptotic cells, and other foreign particles [Leverrie et al., 2001; May and Machesky, 2001; Lee et al., 2003]. Phagocytosis triggers the activation of multiple transmembrane signaling pathways, leading to the reorganization of the actin cytoskeleton and the formation of a sealed intracellular compartment, the phagosome [Tjelle et al., 2000]. The newly formed phagosome undergoes a maturation process by a series of fusions with endocytic compartments and eventually lysosomes, and finally kills and degrades ingested substances within the phagolysosome [Desjardins et al., 1994; Tjelle et al., 2000]. The coordinated maturation of phagolysosomes by the acidification and recruitment of hydrolases [Griffiths, 2004] is crucial for its microbicidal action [Hackam et al., 1997] and the degradation of phagosomal content [Grinstein et al., 1992]. A low pH by itself is lethal for many microorganisms and also provides an optimal condition for the activation of lysosomal hydrolytic enzymes [Hackam et al., 1997]. It was previously shown that vacuolar-type ATPases (V-ATPases) accumulate in the phagosomal membrane during maturation [Hackam et al., 1997; Tsukano et al., 1999], and was, thus, thought to be the crucial determinant in phagosome acidification [Hackam et al., 1997]. In macrophages, V-ATPases are involved in the killing of bacteria and senescent erythrocytes [Grinstein et al., 1992]. It was shown that proteases and other lysosomal hydrolases become active to kill ingested pathogens when the pH within phagolysosomes (late phagosomes) reaches 5.0 [Lee et al., 2003]. The fusion of phagosomes with lysosomes or other endocytic vesicles is microtubule dependent and a prerequisite for phagosome maturation because they facilitate fusion between phagosomes and organelles of the endocytic pathway [Blocker et al., 1996]. Besides professional phagocytes from higher eukaryotes, some unicellular organisms, such as the slime mold, *Dictyostelium discoideum*, and an enteric parasite, *Entamoeba histolytica*, show an inherent phagocytosis ability. *Entamoeba histolytica*, a potentially invasive enteric protozoan parasite, causes an estimated 50 million cases of amebiasis: amebic colitis, dysentery, and extraintestinal abscesses [Petri, 2002], and 40,000–100,000 deaths annually [WHO/Pan American Health, 1997]. The trophozoite of *E. histolytica* colonizes the human gut and engulfs foreign cells, including microorganisms and host cells. During tissue invasion, the trophozoite first depletes the mucus of the intestinal parenchyma and then kills and phagocytoses the underlining host cells [Ravdin et al., 1980]. A related *Entamoeba* species, which is morphologically indistinguishable from *E. histolytica* and shows 95% similarity to *E. histolytica* within the protein coding sequences at the nucleotide level [Willhoeft et al., 2000], also colonizes the human gut and ingests microorganisms for its nutritional requirements. However, when humans are infected with *E. dispar*, the trophozoites remain as a harmless commensal in the bowl lumen, without causing local invasion leading to dysentery and liver abscesses. As these two amoebas are similar in their genetic background, cell biology, and host range, the systematic comparison between *E. histolytica* and *E. dispar* constitutes an important area of research to identify and analyze the factors that might be important for its amebic pathogenicity [Horstmann et al., 1992].

It has been demonstrated that the ability of ingesting and killing microorganisms and their host cells [Huston et al., 2003] is closely associated with an amoeba's pathogenesis. It was previously shown that mutants deficient in phagocytosis were avirulent both in vitro and in vivo [Orozco et al., 1983]. A number of amebic proteins involved in phagocytosis and virulence were previously identified, including galactose/*N*-acetylgalactosamine-inhabitable lectin [Petri, 2002], cytoskeletal proteins, and their associated regulatory molecules [Voigt et al., 1999], cysteine proteases (CP) [Bruchhaus et al., 1996; Que and Reed, 2000], pore-forming peptides (i.e., amoebapores)[Leippe et al., 1994], and Rab GTPases [Saito-Nakano et al., 2004]. Most of these proteins and their encoding genes are present in both *E. histolytica* and *E. dispar* with few exceptions, e.g., CP1 and CP5 [Bruchhaus et al., 1996]. The morphological differences of phagosomes between the two species have recently been demonstrated [Pimenta et al., 2002]. *E. histolytica* contained multiple bacteria in their phagosomes, whereas phagosomes in *E. dispar* contained a sin-

gle bacterium and some bacteria were freely present in the cytoplasm (i.e., not enclosed by the membrane structure) [Pimenta et al., 2002]. However, since the *E. histolytica* and *E. dispar* xenic strains used in the study were cultivated with uncharacterized and likely different bacterial flora [Pimenta et al., 2002], it was not clear that the observed differences in phagosome morphology were attributable to inherited differences in the phagosome structures and biogenesis between the two species or to different culture conditions, e.g., co-cultured bacteria species. In the present study, we examined morphological differences of phagosomes containing a homogeneous (not a mixture) line of *Pseudomonas aeruginosa*, using electron and light microscopes. In addition, we demonstrated the differences in the kinetics of phagosome maturation, with video microscopy, between the axenically cultivated *E. histolytica* and *E. dispar* strains.

MATERIALS AND METHODS

Chemicals

All chemicals of analytical grade were purchased from Wako (Tokyo, Japan) unless otherwise stated. Concanamycin A, nocodazole, 2,3-butanedione monoxime (BDM), and trans-epoxysuccinyl-L-leucylamido-(4-guanidino) butane (E64) were purchased from Sigma-Aldrich (Tokyo, Japan). 3,5-Dinitro-N^4, N^4-dipropylsulfanilamide (Oryzalin) was purchased from AccuStandard (New Haven, CT). Latrunculin A was purchased from Molecular Probes (Eugene, OR).

Cultivation of Parasites, Bacteria, and Yeast

Trophozoites of *E. histolytica* HM-1: IMSS cl6 were cultured axenically in BI-S-33 as previously described [Diamond et al., 1972]. *E. dispar* CYNO 09: TPC [Kobayashi et al., 1998] were cultured in YIGADHA-S medium, as described [Diamond et al., 1978; Kobayashi et al., 2000]. Promastigotes of green fluorescence protein (GFP)-expressing *L. amazonensis* [Chan et al., 2003], a gift from K. P. Chang and S. Kawazu, were cultured in 199 medium (Nissui Pharmaceutical, Tokyo, Japan) supplemented with 10% heat-inactivated fetal calf serum, 25 mM HEPES and 5 μg/ml tunicamycin. *Pseudomonas aeruginosa* PA: KEIO strain [Nozaki et al., 1999] was cultivated in BI-S-33 medium at 35°C. GFP-expressing *Saccharomyces cerevisiae* [Sato et al., 2001], a gift of Koichi Nihei and Akihiko Nakano, Riken, was grown in MCD medium containing 0.67% yeast nitrogen base without amino acids, 2% glucose, and 0.5% casamino acids (Difco, Detroit, MI).

Phagocytosis Assays

Approximately 5×10^4 trophozoites were seeded on a 0.79-cm^2 well of a collagen-coated glass-bottom culture dish (MatTek Corporation, Ashland, MA), mixed with 1×10^6 fluorescein isothiocynate (FITC)-labeled yeasts, GFP-expressing yeasts or GFP expressing-*L. amazonensis* (1:20), enclosed with a cover slip, and further cultured at 33°C in a temperature control unit on an AS Multi Dimension Workstation (AS-MDW, Leica Microsystems, Wetzlar, Germany). At 20 min, 6–8 images (~40–50 trophozoites/image) were captured under on a DM IRE2 inverted microscope with a HC PLAN APO 20×/0.70 objective (Leica) integrated in a Leica AS-MDW system, and the internalized cells were counted manually.

Measurement of Phagosome pH

Phagosome pH was measured by ratiometry using FITC-conjugated yeasts as previously described [Ohkuma and Poole, 1978]. It has been shown that the fluorescence spectrum of FITC changes as a function of pH and is not affected by the FITC concentration (i.e., the FITC-labeling efficiency of yeasts), ionic strength, or associated proteins (i.e., constituents of the media used or the content of phagosomes) [Ohkuma and Poole, 1978]. FITC-yeasts (5×10^5; Molecular Probes, Eugene, OR) were suspended in 75% PBS and 25% BI-S-33 or YIGADHA-S medium supplemented with 137 mM L-cysteine and 19 mM ascorbic acid and adjusted to pHs ranging from 4.0 to 7.5, transferred to a collagen-coated glass-bottom dish and covered with a cover slip. Fluorescence and phase contrast images of 10 continuous slices (z-stack) with 1-μm intervals of FITC-yeasts were acquired with a Roper Cool Snap HQ digital camera (Roper Scientific, Duluth, GA) at two excitation wave lengths (495 and 440 nm) on the system described above with a BGR filter (#11513838). After the best focused particles were manually chosen, the fluorescence intensities with two excitation wavelengths of the 1.3 μm^2-circular region of interest (ROI) within a particle were measured. The fluorescence signal of four ROI per particle of 20 randomly selected particles was determined at each pH value. After the background fluorescence signal intensities were subtracted, the ratio of the fluorescent signal excited at 495 nm to that excited at 440 nm was plotted against the pH value to obtain a standard curve. For the measurement of phagosome pH, all experiments using live trophozoites were performed using the same mixture as mentioned above. For the short-term phagosome acidification, ~5×10^4 trophozoites were seeded on the collagen-coated glass-bottom culture dish, mixed with FITC-yeasts (5×10^5), enclosed with a cover slip, and further cultured at 33°C. Time-lapse video micro-

scopy was performed at an interval of 30 s for 3 h and ingested single FITC-yeast containing trophozoites were selected, and the pH was measured using the standard curve created above. For long-term phagosome acidification, trophozoites (1×10^6) were settled in the wells of a 12-well cell culture plate (Corning Incorporated, Corning, NY) at 35°C for 30 min, gently mixed with FITC-yeast (5×10^7), sealed the plate, centrifuged for 5 min at 500*g* for artificial internalization of yeast, washed to remove noninternalized particles, and cultured again in a collagen-coated dish at 33°C. Time-lapse video microscopy was performed for 12 h at 30 min intervals, and the pHs of 20–30 ingested particles were measured as mentioned above.

Degradation of GFP-Yeasts and GFP-*L. amazonensis*

Approximately 5×10^4 trophozoites of *E. histolytica* or *E. dispar*, settled on the collagen-coated glass-bottom culture dish, were mixed with 5×10^5 GFP-yeasts or GFP-*L. amazonensis* at a ratio of 1:10 and cultivated as described above. Time-lapse video microscopy was performed with a Leica AS MDW system as described above. The fluorescence intensity of the whole GFP-yeasts or GFP-*Leishmania* with an excitation at 489 nm with the GFP filter (#11513852) was measured by quantifying the intensity within manually drawn ROI of the maximum projection images captured at 15–30 s intervals for 2.5 h.

Treatment of Parasites With Inhibitors

To test the effects of phagosome acidification and degradation, ~4–6 $\times 10^5$ trophozoites of *E. histolytica* or *E. dispar* were pretreated for 1 h with 10 μM concanamycin A, a specific inhibitor for V-ATPase; 20–200 μM of nocodazole, 100–200 μM of oryzalin, inhibitors for microtubule polymerization [Makioka et al., 2000], 0.25–0.50 μM of latrunculin A, an inhibitor of actin polymerization [Makioka et al., 2001] or 20–40 mM of BDM, an inhibitor of myosin ATPase [Borlak and Zwadlo, 2004] or 200 μM of E64, a CP inhibitor in 13 × 100 mm^2 screw-capped Pyrex glass tubes at 35°C in BI-S-33 or YIGADHA-S medium, respectively.

Electron Microscopy

E. histolytica and *E. dispar* trophozoites were harvested, washed, and resuspended in BI-S-33 and YIGADHA-S medium, respectively. The concentrations of trophozoites were maintained at ~1×10^5 cells/ml in 13 × 100 mm^2 screw-capped Pyrex glass tubes. The trophozoites were then incubated with 300 μl of a logarithmic culture of *P. aeruginosa* at 35°C for 18 h, washed three times with PBS, pH 7.4, containing 2% glucose, followed by centrifugation at 1500*g* for 2 min. The cell pellet was resuspended and prefixed with 2% glutaraldehyde in PBS for 1 h. After rinsing, the samples were postfixed with 1% OsO_4 in PBS for 1 h, stained en bloc with 1% uranyl acetate, dehydrated in a graded series of ethanol, and embedded in Epon 812 (TAAB Laboratories Equipment, England). Ultrathin sections were made on an LKB-ultramicrotome (LKB-Produkter, Sweden). Sections were stained with uranyl acetate and lead citrate and examined with a Hitachi-H-700 electron microscope.

RESULTS

Morphological Differences of *P. aeruginosa*-containing Phagosomes Between Pathogenic and Nonpathogenic *Entamoeba* Species

To examine the morphological differences of phagosomes between pathogenic and nonpathogenic *Entamoeba* species, trophozoites of *E. histolytica* and *E. dispar* were cultivated with *P. aeruginosa* for 18 h and examined under electron and light microscopes. Both *E. histolytica* (Fig. 1 A and 1C) and *E. dispar* (Fig. 1B, 1D, and 1E) trophozoites showed the general ultrastructural architecture common to this group of parasites, as previously described [Lushbaugh and Miller, 1988; Espinosa-Cantellano et al., 1998; Pimenta et al., 2002]. The cytoplasm lacks a typical rough endoplasmic reticulum, Golgi apparatus, and mitochondria. The cytoplasm of both species was filled with vesicles and vacuoles varying in size. Some of these vacuoles contained ingested bacteria and degraded bacterial debris. Ingested bacteria were always found to be enclosed within the phagosome membrane in both species, which contradicts the previous report [Pimenta et al., 2002]. We failed to count the bacteria ingested by the trophozoites using DAPI staining, as the ingested bacteria in the *E. histolytica* phagosomes were often degraded and, consequently, some phagosomes were evenly stained with DAPI (Fig. 2A). We thus examined the number of bacteria ingested by the trophozoites on electron micrographs where the membrane structures were still recognizable after disintegration of the bacterial cell membrane (Fig. 1). *E. histolytica* trophozoites ingested a greater number of bacteria (56.0 ± 15.5) than *E. dispar* (45.5 ± 2.1) [mean ± standard deviation (S.D.)] per cell. The average number of bacteria per phagosome in *E. histolytica* and *E. dispar* was 2.45 ± 0.07 and 1.74 ± 0.38, respectively ($p<0.05$ with Students *t*-test). The numbers of phagosomes containing greater than four bacteria were higher in *E. histolytica* than in *E. dispar* (5% and 14%, respectively) (Fig. 2E). In *E. histolytica*, 5% of phagosomes contained more than seven bacteria, while no phagosome contained more than seven bacteria in *E. dispar* (data not shown). The average diameter of phagosomes was slightly higher in *E. histolytica* than in *E. dispar*

J_ID: Z7W Customer A_ID: 05015 Cadmus Art: CM0721 Date: 26-JULY-05 Stage: I Page: 5

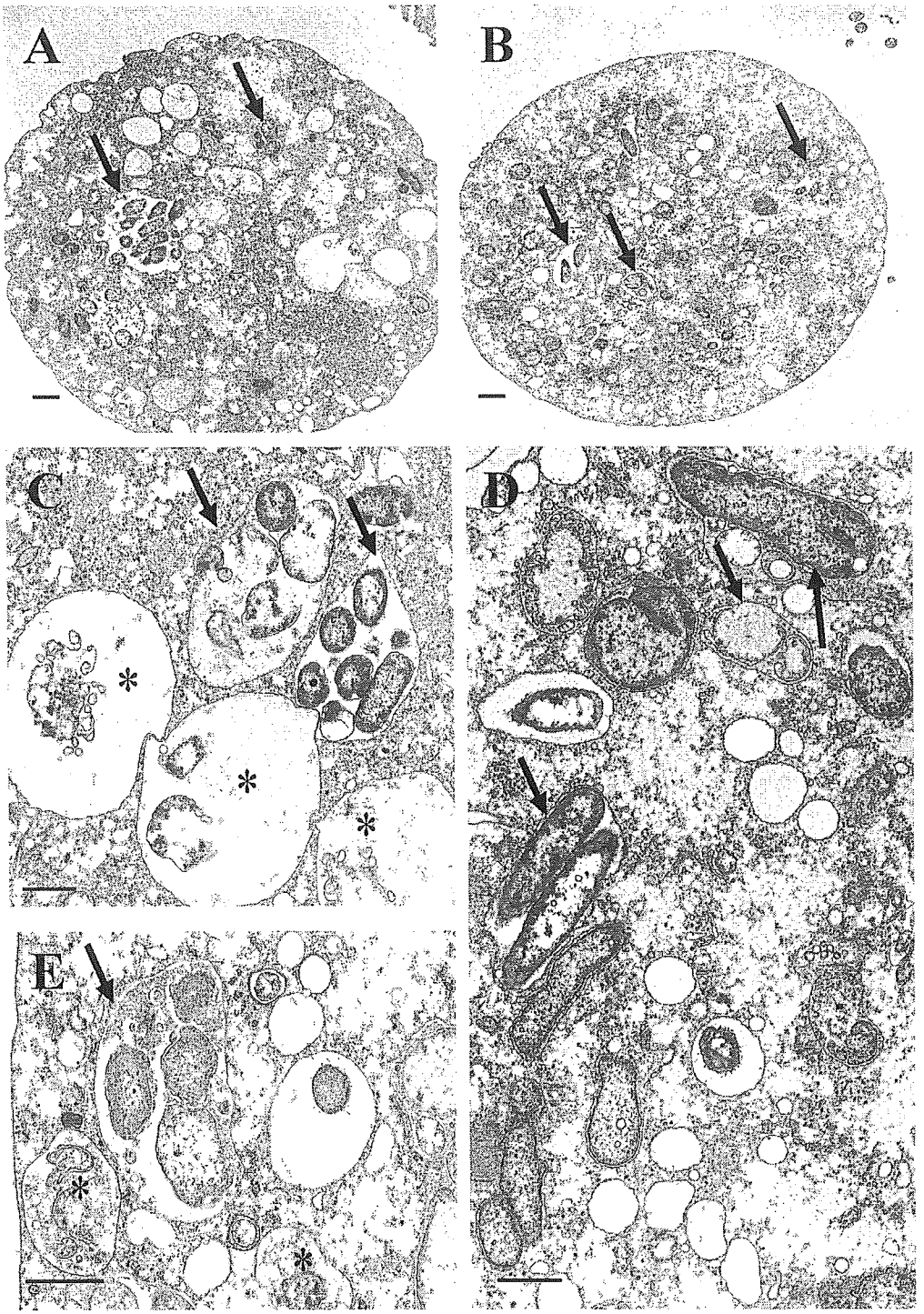

Fig. 1. Electron micrographs of phagosomes in *E. histolytica* (**A** and **C**) and *E. dispar* trophozoites (**B**, **D**, and **E**) cultivated with *P. aeruginosa*. The arrows indicate phagosomes containing multiple bacteria in both species. Asterisks show phagosomes containing degraded *P. aeruginosa* in *E. histolytica* (C) and *E. dispar* (E). Bars indicate 1 μm.

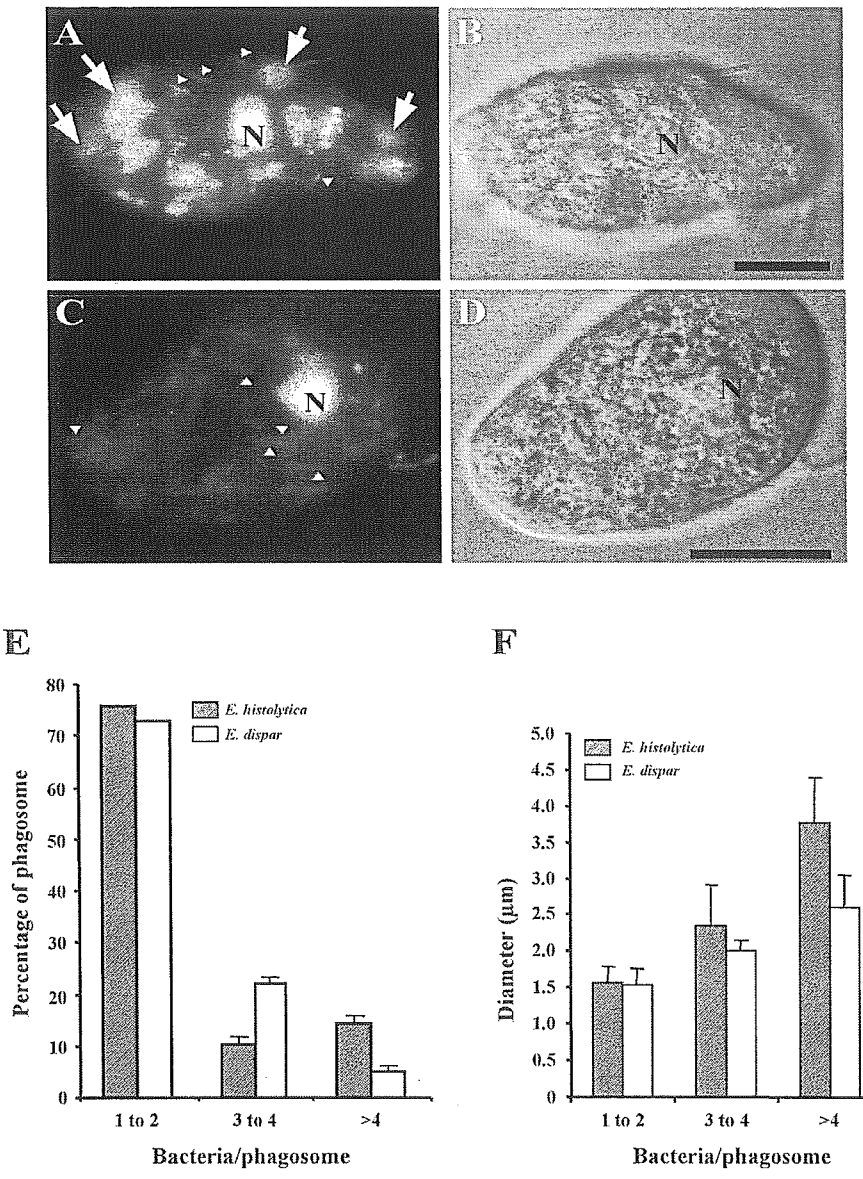

Fig. 2. Qualitative (**A–D**) and quantitative (**E**, **F**) differences in the ingestion and degradation of bacteria between the two *Entamoeba* species. A–D: Light microscopic images of *E. histolytica* (A, B) and *E. dispar* (C, D) trophozoites that ingested bacteria and were stained with DAPI (A, C). Phase images are also shown (B, D). Note that, in *E. histolytica* trophozoites, the majority of bacteria in phagosomes were lysed and many phagosomes were evenly stained with DAPI (arrows), whereas, in *E. dispar* trophozoites, most of the ingested bacteria remained a partially intact (arrowheads). Nuclei are depicted with "N". Bars represent 10 μm. E–F: The number of bacteria ingested per phagosomes (E) and the average size of phagosomes (F) in *E. histolytica* (cross-hatched bars) and *E. dispar* (open bars) are shown. Error bars represent S.D. of the measurement of 120–170 phagosomes.

(Fig. 2F). This was mainly due to the difference in the average number of bacteria ingested by these two species, because the average diameter of phagosomes similarly increased in both types of amoebae as the number of bacteria/phagosome increased.

Light microscopic observation of the DAPI-stained trophozoites also revealed that bacteria in the *E. histolytica* phagosomes appeared to be degraded extensively (Fig. 2A–2B). A large proportion of phagosomes were evenly stained and the morphology of the ingested bacteria was no longer recognizable (arrows), while a majority of ingested bacteria in *E. dispar* phagosomes retained their cell morphology (Fig. 2C, arrowheads; also in *E. histolytica* Fig. 2A).

Comparison of Phagocytosis of Fixed FITC-Yeast, Live GFP-Yeast, and GFP-*L. amazonensis*

We compared the efficiency of internalization of a number of natural and inert particles, i.e., chemically-fixed FITC-conjugated yeasts, live GFP-yeasts, GFP-*L. amazonensis* promastigotes, erythrocytes, and fluorescent beads, between *E. histolytica* and *E. dispar*. Live GFP-*Leishmania* promastigotes were most efficiently ingested among these particles (Fig. 3) (data of erythro- F3